DEVELOPMENT OF A FRAMEWORK FOR COMPOUND FLOODING RISK ASSESSMENT DUE TO TSUNAMI AND HIGH RIVER FLOW

Reo Minami[1], Masaya Toyoda[1], Shigeru Kato[1], Nobuki Fukui[2], Takuya Miyashita[3], Nobuhito Mori[3], Sooyoul Kim[4]

Abstract:

Composite flooding hazards were evaluated using a tsunami–flood coupled model for Mikawa Bay, Aichi Prefecture. Using eleven tsunami patterns provided by the Central Disaster Prevention Council, we performed calculations for 55 events considering five river-flow patterns (base runoff, 25, 50, 75, and 100%) in a tsunami scenario based on the most recent flood case of June 2023. The water levels of six rivers calculated using the distance from the river mouth were at peak on the river mouth when flooding was small (base runoff, 25%), and the maximum level occurred approximately 2.0 km upstream from the river mouth. Additionally, the characteristics of water level rise between the rivers in response to the composite hazard (difference between the most recent flood and base runoff) were at peak (+4.8 m) in the Otowa River and at minimum (+1.2 m) in the Umeda River. Based on the above measurements, we clarified the influence of river flow on tsunami and spatial characteristics.

Keywords: compound flooding, tsunami, river flood, tsunami river run-up, numerical modeling

1. INTRODUCTION

In countries such as Japan, where various natural disasters are likely to occur, it is necessary to consider the possibility of multiple disasters occurring simultaneously or consecutively (compound disasters) when considering the worst-case scenario of an earthquake. In particular, in the eastern part of the Aichi Prefecture, located relatively close to the assumed epicenter of the Nankai Trough earthquake, urban areas have formed around the mouths of rivers of various sizes. In this region, damage estimates for earthquakes and tsunamis (Toyohashi City, 2014) and assessments of compound disasters due to storm surges and floods caused by typhoons have been conducted by Toyoda et al.(2024), but none have considered the river run-up of tsunamis in detail. In the inundation estimates conducted by the government (Cabinet Office Central Disaster Prevention Council, 2012)

The worst-case flood case during a tsunami was estimated by simple superposition, and the interaction between the river run-up of the tsunami and small- and medium-sized floods was excluded because of the worst-case scenario. The rivers considered were large or rivers with a river mouth discharge of 1000 m^3/s or more. A basin-wide discussion is necessary considering small- and medium-sized rivers within the region.

In the eastern Mikawa region of the Aichi Prefecture, heavy rainfall events that cause flooding occur every year from May to October. In May, July, and September 2022, floods equivalent to the flood danger level occurred in the Umeda River (a small and medium-sized river), and in June 2023, several small rivers flooded simultaneously (Toyohashi City website, 2023). Therefore, it is necessary to assume that a tsunami may occur during the flood season and to evaluate the impact of the river discharge from upstream and the run-up tsunami from the river mouth on water levels. Many reports on compound disasters have been based on storm surges. For example, Kawasaki et al. (2016) conducted an analysis of storm surges and earthquakes in the event of a past typhoon or a historical extreme typhoon after the Nankai Trough mega-earthquake. They pointed out that the amount of crustal deformation after the

[1] Graduate School of Engineering, Toyohashi University of Technology (1-1 Tenpakucho, Toyohashi City, Aichi Prefecture, 441-8580)
[2] Graduate School of Engineering, Nagoya Institute of Technology (Gokiso-cho Showa-ku Nagoya City Aichi Prefecture 466-8555)
[3] Disaster Prevention Research Institute, Kyoto University (Gokasho, Uji City, Kyoto Prefecture, 611-0011)
[4] Center for Water Cycle, Marine Environment, and Disaster Management, Kumamoto University (2-39-1 Kurokami, Chuo-ku, Kumamoto City, Kumamoto Prefecture, 860-8555)

earthquake, the strengthening of typhoons, and the rise in sea level due to global warming were directly linked to the impact of flooding damage around the port area. Additionally, Toyoda et al.(2024) constructed an integrated atmosphere–ocean–river model to evaluate the precipitation and storm surges associated with typhoons by combining meteorological, rainfall-runoff, and wave and storm surge models. Using this framework, they analyzed the simultaneous occurrence of storm surges and flooding during typhoons and reported that the smaller the river, the higher the likelihood of the simultaneous occurrence of storm surges and flooding. However, these studies mainly focused on storm surges and did not adequately assess the impact of tsunamis on small- and medium-sized rivers.

Furthermore, Aoyama et al.(2017) analyzed tsunamis that run up rivers through numerical calculations and model experiments and reported that the accuracy of the calculations for reproducing river run-up depends on the roughness coefficient owing to the shape of the river channel and the magnitude of the RMSE owing to differences in water depth. Nakamura et al.(2017) applied a numerical model based on nonlinear shallow-water equations and confirmed that when a tsunami entering the river mouth becomes nonlinear, mass transport occurs and flows into the river, and the average water level increases over time in the main river and tributaries. These studies focused on the run-up impact of a tsunami alone and did not consider water-level deviations when a certain amount of discharge flows into a river. Tolkova et al.(2012) used a numerical method to predict tsunami propagation along rivers. They concluded that various factors are involved in the intrusion of a tsunami into a river, and, in the case of relatively small-scale tsunami events, the intrusion length correlates well with river mouth characteristics. Furthermore, Kayane et al.(2012) investigated the effect of riverbed gradient on the inflow of tsunamis into rivers by comparing actual measurements with theoretical values and found that the relationship between riverbed gradient and inflow distance tends to decay exponentially. Thus, it is difficult to fully grasp the behavior of tsunamis using unified numerical calculations because the river shape significantly influences the intrusion and inflow characteristics of tsunamis into rivers. Therefore, it is necessary to focus on the mechanism of tsunami intrusion into rivers and river inflow in small- and medium-sized rivers and to increase the number of cases.

We used a numerical model to assess compound disasters and determine the extent of water level rise and dangerous locations in the event of a tsunami or river flood. We constructed a compound disaster framework for tsunamis and river floods by improving the framework for storm surges and floods (Toyoda et al.,2024).

2. COMPUTATIONAL SETTING

This study used JAGURS (Baba et al., 2015) based on a nonlinear long-wave equation for tsunami propagation, the rainfall-runoff-inundation (RRI) model (Sayama et al., 2012), and the wave–storm surge coupled (SuWAT) model (Kim et al., 2008) considering river channels for complex hazard assessment. By improving the complex inundation model proposed by Toyoda et al. (2024) and inputting tsunami information from the boundaries, a compound disaster framework for tsunamis and river floods was constructed.

2.1 Tsunami calculations using JAGURS

First, JAGURS, developed for highly accurate tsunami prediction, was used to simulate the tsunamis flowing into the Ise and Mikawa bays. JAGURS uses a long-wave equation that approximates the equations of motion and continuity as long waves by solving the time evolution using the finite difference method. Thus, it is possible to calculate the propagation of tsunamis from the source to the coast as well as the inundation of land and run-up in rivers. It supports two types of equations: a nonlinear equation that considers the advection term (the amount of change in speed owing to movement in space) and friction on the seabed, and a linear equation that considers neither. The coordinate system used is spherical; therefore, it can perform calculations for tsunamis propagating across the Pacific Ocean (Baba et al., 2017). In this study, calculations were performed using Cartesian coordinates.The governing equations used in JAGURS are belows.

The nonlinear long wave equations that form the basis of the numerical model are shown in equations (1) to (3). The equation consists of a continuity equation derived from the law of conservation of mass and an equation of motion derived from the law of conservation of motion. The explanations of

the equations are taken from the “Guide for Establishing Tsunami Inundation Assumptions” issued by the Ministry of Land, Infrastructure, Transport and Tourism of Japan.

$$\frac{\partial \eta}{\partial t}+\frac{\partial M}{\partial x}+\frac{\partial N}{\partial y}=0 \tag{1}$$

$$\frac{\partial M}{\partial t}+\frac{\partial}{\partial x}\left(\frac{M^2}{D}\right)+\frac{\partial}{\partial y}\left(\frac{MN}{D}\right)=-gD\frac{\partial \eta}{\partial x}-\frac{gn^2}{D^{7/3}}M\sqrt{M^2+N^2} \tag{2}$$

$$\frac{\partial N}{\partial t}+\frac{\partial}{\partial x}\left(\frac{MN}{D}\right)+\frac{\partial}{\partial y}\left(\frac{N^2}{D}\right)=-gD\frac{\partial \eta}{\partial y}-\frac{gn^2}{D^{7/3}}N\sqrt{M^2+N^2} \tag{3}$$

where η is the change in water level from the still water surface, D is the total depth from the bottom to the water surface, g is the acceleration of gravity, n is Manning's roughness coefficient, and M and N are the total flow fluxes in the x and y directions, given by equations (4) and (5) by integrating the horizontal velocities u and v from the water bottom h to the water surface η.

$$M=\int_{-h}^{\eta}udz=u(h+\eta)=uD \tag{4}$$

$$N=\int_{-h}^{\eta}vdz=v(h+\eta)=vD \tag{5}$$

Since this is a long wave, the horizontal velocity is assumed to be uniformly distributed in the vertical direction. The first term in the equation of motion is called the local term, the second and third terms are advection terms (nonlinear terms), the fourth term is the pressure term, and the fifth term is the bottom friction term.

JAGURS uses multilevel nesting to perform calculations with increased grid resolution for specific regions within the calculation domain. All 11 patterns proposed by the Cabinet Office Central Disaster Prevention Council (Cabinet Office Central Disaster Prevention Council, 2012) were used as tsunami fault parameters (Table 1). The JAGURS calculation domain was configured with four levels of nesting from 810 m (D1) to 30 m (D4). The results of D4 were set to confirm the effects of reflected waves from land, and it was confirmed that the effect of reflected waves on the final water-level deviation was minimal at approximately a few centimeters. The calculation results for D3 were used as the boundary conditions for the SuWAT model (Figure 1). The physical quantities used as boundary conditions were the flow velocity and water level extracted at 2-min intervals. Tidal conditions were not considered in this calculation, and the tsunami height was considered as the water-level deviation based on the start of the calculation (Table 2a).

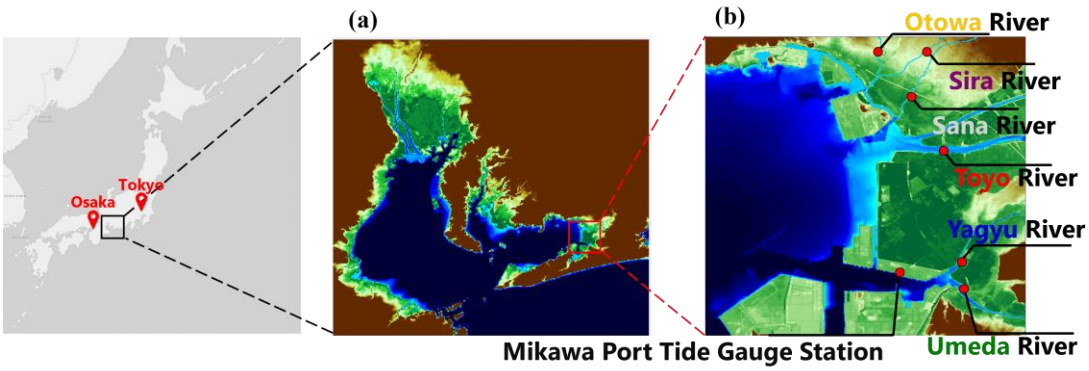

Figure 1. Computational domains of (a) JAGURS and (b) SuWAT in a multi-hazard framework study

Table 1. Cabinet Office Central Disaster Prevention Council tsunami patterns

Tsunami pattern	Large and ultra-large slide areas	
	Position	Location of slip area
Chubo01	Suruga Bay to Kii Peninsula	Large + extra-large slip area
Chubo02	Kii Peninsula	
Chubo03	Kii Peninsula to off the coast of Shikoku	
Chubo04	Off the coast of Shikoku	
Chubo05	Off the coast of Shikoku to off the coast of Kyushu	
Chubo06	Suruga Bay to Kii Peninsula	Large slip + (ultra-large slip area, splay fault)
Chubo07	Off the coast of Kii Peninsula	
Chubo08	Suruga Bay to Eastern Aichi Prefecture, Off the coast of southern Mie Prefecture to off the coast of Tokushima Prefecture	Large + extra-large slip area
Chubo09	Off the coast of Aichi Prefecture to off the coast of Mie Prefecture, Cape Muroto	
Chubo10	Off the coast of southern Mie Prefecture to off the coast of Tokushima Prefecture, Cape Ashizuri	
Chubo11	Cape Muroto, Hinata nada	

Table 2a. JAGURS model conditions

Timestep (s)	0.2
Calculation period (s)	21600
Output interval (s)	600
Response time (s)	10
Roughness coefficient ($m^{-1/3}s$)	0.025

Table 2b. RRI model conditions

	Toyo	Umeda	Yagyu	Otowa (Sira)	Sana
Simulation period	2023/05/30 00:00–2023/06/04 00:00 UTC				
Resolution (arc-sec)	3	1			
Time step (s)	600				
River roughness ($m^{-1/3}s$)	0.0275				
Base flow (m^3/s)	5.00	1.45	0.23	1.69	1.02
River width (m)	50–100	23	11.7	25 12	20
Number of observation points in transverse direction	-	23	12	25 12	20
Step size (m)	-	10	1.0/0.7	1.0	1.0
Riverbed gradient	1/8400–1/780	1/2000–1/400	1/560	1/500–1/100	1/1300–1/315
Embankment height (m)	7.00	4.40	4.10	4.00	4.00

2.2 Flow calculation using the RRI model

The RRI model was used to represent the river flow caused by rainfall. This model is capable of calculating the flow of an entire river system based on the spatiotemporal distribution of precipitation and topographical data (Table 2b) and is a two-dimensional model that can analyze not only river flow but also flooding by inputting rainfall. The model is divided into two parts: the river channel and the

slope that contacts the channel. It considers lateral groundwater flow in mountainous areas and vertical infiltration in flat areas. The two-dimensional shallow water equations that form the basis of the RRI model were derived based on the mass balance and motion equations shown below for unsteady river flow. Refet to the the RRI Use Manual for further detail. The governing equations can be descrived as follows:

$$\frac{\partial h}{\partial t}+\frac{\partial q_x}{\partial x}+\frac{\partial q_y}{\partial y}=r-f \tag{6}$$

$$\frac{\partial q_x}{\partial t}+\frac{\partial u q_x}{\partial x}+\frac{\partial v q_x}{\partial y}=-gh\frac{\partial H}{\partial x}-\frac{\tau_x}{\rho_w} \tag{7}$$

$$\frac{\partial q_y}{\partial t}+\frac{\partial u q_y}{\partial x}+\frac{\partial v q_y}{\partial y}=-gh\frac{\partial H}{\partial y}-\frac{\tau_y}{\rho_w} \tag{8}$$

Here, h is the water depth, q_x and q_y are the flow fluxes in the x and y directions, respectively, ($q_x = uh,\ \ q_y = vh$), u and v are the flow velocities in the x and y directions, respectively, r is the rainfall intensity, f is the vertical infiltration intensity, H is the water level from the reference point, ρ_w is the water density, g is the gravitational acceleration, and τ_x and τ_y are the shear stresses in the x and y directions, respectively, which are calculated using Manning's law as

$$\frac{\tau_x}{\rho_w}=\frac{gn^2u\sqrt{u^2+v^2}}{h^{1/3}} \tag{9}$$

$$\frac{\tau_y}{\rho_w}=\frac{gn^2v\sqrt{u^2+v^2}}{h^{1/3}} \tag{10}$$

where n denotes the roughness coefficient. The momentum equations were calculated by applying the corresponding equations of motion to mountainous areas where rainwater infiltration is low and to plain areas where water is easily permeable, taking into account the subsurface infiltration rate. The RRI drainage basin was divided into river channels and slopes, and the water gap between the river and slope grid cells was calculated at each time step from the relationship between the height of the slope water, river water, and levee. A diffusion wave approximation model similar to that for the slopes was used for the river channels. However, river channels were treated as one-dimensional. The river channel cross-section was assumed to be rectangular, and the river channel width, depth, and levee height were provided in the river channel grid cells to specify the shape of the river channel cross-section. If detailed river channel cross-sectional information could not be obtained, the river channel width and depth were calculated as a function of the catchment area as a first approximation as

$$w=C_wA^{S_w} \tag{11}$$

$$D=C_DA^{S_D} \tag{12}$$

where A [km^2] is the catchment area of the river channel section. The units of w and D are [m]. The river channel parameters C_w, S_w, C_D, and S_D were estimated from the cross-sectional information available for each target basin. When setting the levee height, water exchange was not necessary if it was greater than the water level of the river channel and slope; otherwise, the overflow volume was calculated as

$$q_{rs}=\begin{cases}\mu_2h_1\sqrt{2gh_1} & h_2/h_1\le 2/3\\ \mu_3h_2\sqrt{2g(h_1-h_2)} & h_2/h_1>2/3\end{cases} \tag{13}$$

where μ_2 and μ_3 are constant coefficients (0.35, 0.91), and h_1 indicates the difference between the river water level and the levee height. The Runge–Kutta formula was applied to the time step.

The six target rivers were Toyo, Yagyu, Umeda, Otowa, Sira, and Sana. We first performed a calculation to reproduce the river discharge during the extreme precipitation on June 2, 2023, the most recent flood event. We used Ministry of Land, Infrastructure, Transport, and Tourism XRAIN data provided by DIAS (horizontal resolution: 250 m, 10-min intervals), and J-Flw Dir(Yamazaki et al.,2018) was used as topographical data (horizontal resolution, 30 m). To confirm the water-level deviation due to tsunamis and floods according to the flood scale, we assumed five flood cases considering the river discharge owing to extreme precipitation as 100% and river discharge values of 25, 50, and 75% and the base runoff (0%) of each river system. In the RRI model, the river discharge value of the grid point corresponding to the connection point with the SuWAT model was used as the boundary condition. The river flow data (flow value at the boundary point of the SuWAT model (the upstream end of the river in the calculation domain)) were set such that the maximum river flow coincided with the maximum tsunami wave height.

Table 2c. SuWAT model conditions

Inundation calculation "ON"	
Lateral boundary conditions	Tsunami: JAGURS, River discharge: RRI
Input frequency at boundary	Tsunami: 2 min, River discharge: 10 min
Number of meshes	366(i) * 369(j) = 135,054
Horizontal resolution (m)	30
Timestep (s)	1
River flood scenarios (%)	0, 25, 50, 75, 100

2.3 Assessing complex floods using SuWAT

To evaluate the compound hazards of tsunamis and floods in the eastern part of Mikawa Bay, we adopted a SuWAT model, which considers river flow as a compound disaster model and considered the impact of tsunamis and upstream floods (Figure 2). SuWAT combines a planar 2D storm surge model and a simulating waves nearshore (SWAN) model and applies a nesting method using a message-passing interface to estimate storm surges, waves, and flooding quickly and with high accuracy (Kim et al., 2015).

The SuWAT model can calculate any number of subdomains simultaneously. The storm-surge model includes tides, the wetting and drying processes of tidal flats, and radiation stress caused by waves. The basic equations are depth-integrated nonlinear shallow water equations. The explanations in this section are provided in the SuWAT Manual.

$$\frac{\partial \eta}{\partial t} + \frac{\partial M}{\partial x} + \frac{\partial N}{\partial y} = 0 \tag{14}$$

$$\frac{\partial M}{\partial t} + \frac{\partial}{\partial x}\left(\frac{M^2}{d}\right) + \frac{\partial}{\partial y}\left(\frac{MN}{d}\right) + g\,d\frac{\partial \eta}{\partial x} = fN - \frac{1}{\rho_w} d\frac{\partial P}{\partial x} + \frac{1}{\rho_w}(\tau_s^x - \tau_b^x + F_x) + A_h\left(\frac{\partial^2 M}{\partial x^2} + \frac{\partial^2 M}{\partial y^2}\right) \tag{15}$$

$$\frac{\partial N}{\partial t} + \frac{\partial}{\partial x}\left(\frac{NM}{d}\right) + \frac{\partial}{\partial y}\left(\frac{N^2}{d}\right) + g\,d\frac{\partial \eta}{\partial y} = -fM - \frac{1}{\rho_w} d\frac{\partial P}{\partial y} + \frac{1}{\rho_w}\left(\tau_s^y - \tau_b^y + F_y\right) + A_h\left(\frac{\partial^2 N}{\partial x^2} + \frac{\partial^2 N}{\partial y^2}\right) \tag{16}$$

where η is the sea surface height, M and N are the depth-integrated velocity components in the x and y directions, respectively, P is atmospheric pressure, f is the Coriolis parameter, g is the acceleration of gravity, d is the total water depth ($\eta + h$), A_h is the horizontal eddy diffusivity, ρ_w is the water density,

and F_x and F_y are the components of the wave-induced radiation stress. These equations were spatially and temporally discretized on an interleaved Arakawa C grid using the leapfrog method, a finite-difference scheme that uses an upwind method.

The horizontal resolution of the SuWAT calculation setting was 30 m, the sluice gates and culverts were set to fully closed conditions, and the output interval was set to 1 min (Table 2c). The calculation results of JAGURS and RRI were used as the lateral boundary conditions, and the pressure and wind fields were ignored. Furthermore, in the calculation domain set, points more than 2 km upstream were significantly affected by the lateral boundary conditions at the upstream end of the river; therefore, 2 km was set as the farthest upstream point. The calculation period was set to 6 h after the occurrence of a tsunami in the Pacific Ocean, and a sensitivity analysis was performed on 55 cases, including 11 tsunami patterns and five flood patterns.

As mentioned above, three types of calculation models were used. The JAGURS was used to extract the tsunami flow velocity and water level from the calculation results at 2-min intervals which were input from offshore Mikawa Bay as lateral boundary conditions interpolated at 30-m intervals. RRI calculations were performed for the rainfall-runoff of the entire river system, and river flow values for grid points corresponding to the river mouth were extracted at 10-min output intervals. River flow data were input into the SuWAT for two cases: the base runoff (tsunami only) and the maximum river flow adjusted to coincide with the maximum tsunami wave height (compound disaster). Figure 2 shows the simulation flow.

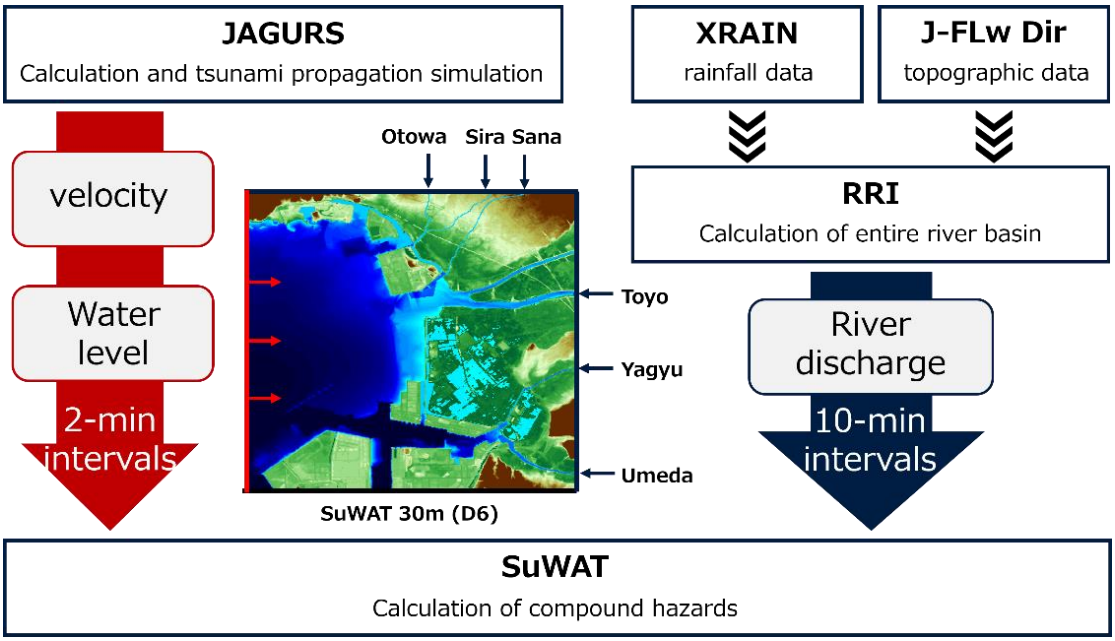

Figure 2. Simulation flow

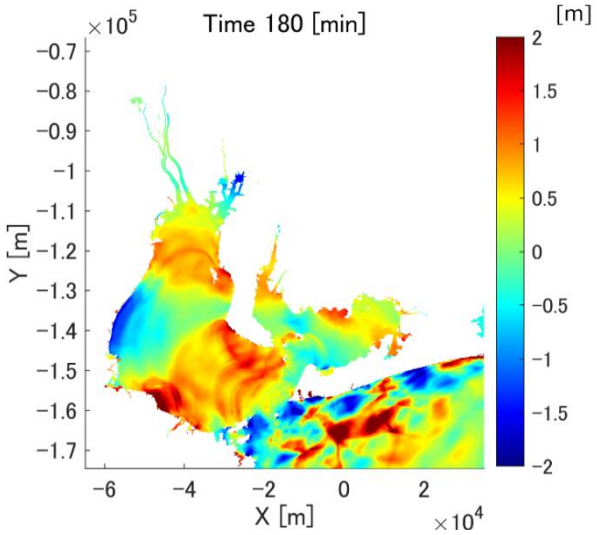

Figure 3. Wave-height distribution by JAGURS (D3) at Chubo01 (180 min after earthquake)

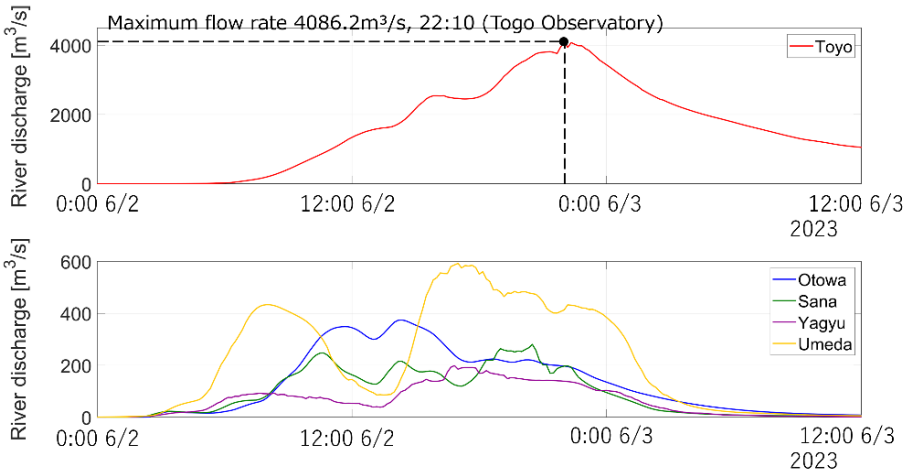

Figure 4 Time series of flow discharge reproduction calculation results using RRI

3. RESULTS AND DISCUSSION

3.1 Validation of tsunamis

The JAGURS tsunami calculations for the 11 cases the Cabinet Office Central Disaster Prevention Council assumed showed that the highest wave height was recorded at Mikawa Port in the eastern part of Mikawa Bay in Chubo01 (approximately 1.9 m). In the tsunami caused by the Nankai Trough earthquake, the maximum wave height in the calculation domain exceeded 10 m. However, in the vicinity of Mikawa Port in Mikawa Bay, the maximum wave height was approximately 2 m. As shown in previous reports (Cabinet Office Central Disaster Prevention Council, 2013), most of the generated tsunami flowed into Ise Bay because the tsunami that split off on the coast west of Ise Bay connected into Mikawa Bay, which is highly closed.

In Chubo01, the large and very-large slide areas were set in “Suruga Bay to the offshore Kii Peninsula.” At Mikawa Port, the interval between the first and second waves was narrow, and the wave height in the bay increased owing to the influence of waves reflected from the coast of Tsu City, Mie Prefecture. A large amount of water flowed into Mikawa Port between 180 and 270 min after the earthquake, with the maximum wave height reaching 1.9 m after 180 min (Figure 3). From the above, the results of the

JAGURS calculations are consistent with the data reported by the Aichi Prefecture (water-level deviation of 1.9 m excluding high tide) (Aichi Prefecture,2015), and it was determined that the reproducibility was high. Therefore, tsunami calculation results were used in the composite inundation model.

3.2 Selection of base flow, flood discharge, and application results

A preliminary calculation was performed using the RRI model from 2022 to 2023 (XRAIN was used as the input condition) to calculate the base runoff in small and medium-sized rivers. However, this calculation underestimated the river discharge during periods of no rainfall, resulting in a large deviation from the base runoff information for the Toyo River (Aichi Prefecture, 2005). Therefore, the observed values from hydrological and water quality databases were used as the base runoff for the Toyo River, and the values obtained from field observations of small and medium-sized rivers were used. Field observations were conducted on October 10, 2023, and river discharge observations (current velocity measurement method) were conducted using a portable propeller current meter.

The torrential rain disaster that occurred in the eastern Mikawa region on June 2, 2023, was selected as the most recent river flood case. A river discharge reproduction calculation was performed using the RRI model for each river system (Figure 4). The topographical data and rainfall-runoff parameters used in the RRI model were set according to previous studies. According to the HQ formula provided by the Toyohashi River Office of the Ministry of Land, Infrastructure, Transport, and Tourism's Chubu Regional Development Bureau, the maximum river discharge at this ancient observation station was 4165 m^3/s at 22:40. The observed value is not publicly available as the data are still being examined; therefore, the estimated value of the HQ formula was used. In the reproduction calculation, the maximum river discharge at the same point was 4086.2 m^3/s at 22:10 on June 2, capturing the river discharge trend owing to heavy rain. For second-class rivers, the model reproduced the peaks between 3 pm and 5 pm in the Yagyu River, the two peaks observed in the morning and evening in the Umeda River, and the peak observed at approximately 9 pm in the Sana River. The model was, therefore deemed able to reproduce the phenomenon appropriately.

3.3 Evaluation of water level rise characteristics due to tsunamis and floods

This study discusses the impacts of tsunamis and floods on the eastern reaches of Mikawa Bay. Five flooding patterns of the most recent flood case (base (0%), 25, 50, 75, and 100% flows) were set as the river flow values. The water level rise of the base flow pattern was extracted at 500-m intervals from the river mouth of each river, and a sensitivity analysis was performed for each expected tsunami pattern. Figure 5 shows the relationship between the water level rise due to the flood at that time and the distance from the river mouth (up to 2 km upstream) for all 11 tsunami patterns for each of the five flood patterns where each line is the average value of six rivers. The water level rise was evaluated as the amount of water level rise from the base flow (normal time), and the maximum reachable water level of each river was calculated by adding the normal water depth to the water level rise. First, in the base-runoff results shown in Figure 5a, the water level rise was greatest at the river mouth, and the amount of water level rise decreased further upstream. A difference of approximately 1.0 m was observed between the river mouth and 2 km upstream. The top three tsunami patterns for the rise in water level were Chubo07, 02, and 01. In the 25% flood case results shown in Figure 5b, a difference of approximately 0.3 m was observed between the river mouth and a point 2 km upstream. In that order, the top three tsunami patterns for the rise in water level were Chubo02, 01, and 10. Therefore, when there was no flood or when it was small scale (base and 25% patterns), the water level rise was greatest at the river mouth regardless of the tsunami pattern, and the water level rise due to the tsunami was dominant.

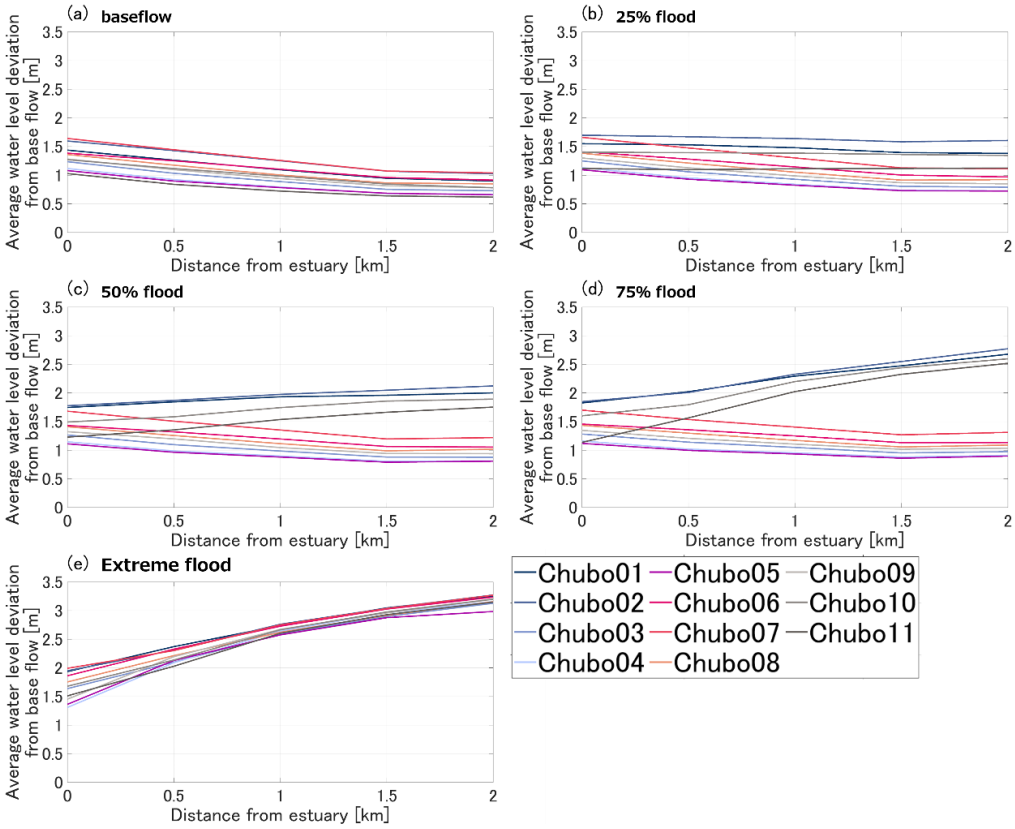

Figure 5. Average water level rise by distance from river mouth for 11 tsunami cases: a) base flow (0%), b) 25% flood, c) 50% flood, d) 75% flood, and e) 100% flood

For the medium-scale 50 and 75% flood patterns, the trend was split in two, with Chubo01, 02, 10, and 11 showing an increase in the water level rising further upstream. Meanwhile, for the base and 25% tsunami patterns, the water-level rise was greater closer to the river mouth (Figures 5c and d). Therefore, in these flood cases, whether the tsunami or flood dominates the rise in water level depends on the combination of tsunami patterns. Furthermore, no particular characteristics were observed in the location of the slide area, and The distance between the epicenter and Mikawa Bay did not affect the results (Figure 5d).

In the results for the most recent flood cases (Figure 5e), the water level rise was greater farther upstream for all assumed tsunami patterns. A maximum change of 2.0 m was confirmed compared with the assumed base runoff for the same tsunami pattern. A difference of approximately 2.0 m in water level rise was also observed between the river mouth and a point 2 km upstream. Based on the tsunami patterns for the top three cases of water level rise, the order was Chubo02, 01, and 07. Meanwhile, at a point 2 km upstream, a difference of 2.4–3.2 m occurred, depending on the combination of the tsunami pattern and flood case. In extreme river flood patterns, the water level rise was significantly higher at the most upstream point.

Next, we compared the maximum water-level deviations for each river. Table 3 lists the maximum water-level deviations (1st place) for all 55 cases and each river during the calculation period. In all rivers, the maximum water-level deviation was the highest among all cases, and the maximum deviation for the five rivers was 2 km upstream from the river mouth. However, the Sana River recorded a maximum water-level deviation of 1.5 km upstream. A detailed analysis of the Sana River is required to determine the cause. The Otowa, Yagyu, and Toyo rivers exhibited the maximum water-level deviations, varying greatly from river to river, ranging from approximately 2 m. In the Otowa River, the flow from the upstream river mouth was strong, and the flow toward the mouth was weak (Figure 6). It was confirmed that the integrated value of the upstream flow velocity during the calculation period was approximately twice that of the Umeda River, which has a similar size. Therefore, it can be concluded that the Otowa River is more susceptible to the influence of both factors (tsunamis and river floods).

Table 3. Maximum water-level deviation for all 55 cases

River	Distance from river mouth (km)	Maximum water-level deviation (m)
Otowa	2.0	4.82
Sira	2.0	2.80
Sana	1.5	2.81
Toyo	2.0	3.40
Yagyu	2.0	3.44
Umeda	2.0	3.17

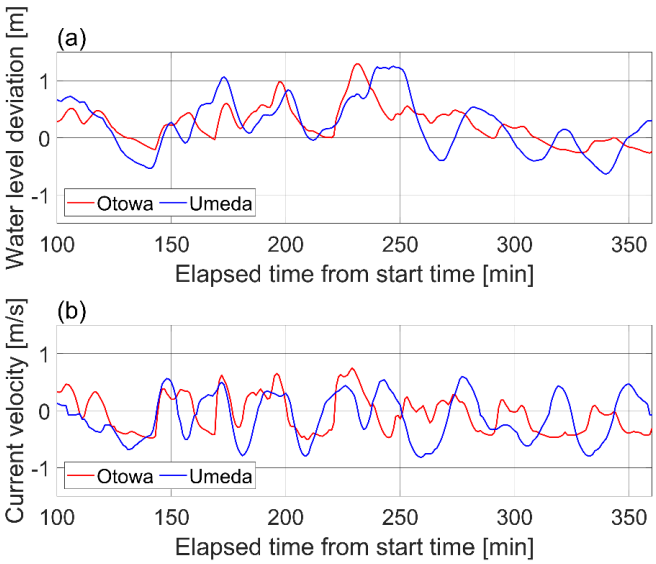

Figure 6. Time series of (a) water-level deviation and (b) current velocity of the Otowa and Umeda rivers at the river mouth in 50% flood case of Chubo01 (red: Otowa River, blue: Umeda River; positive upstream flow velocity)

4. CONCLUSION

A sensitivity analysis was conducted using a compound disaster framework for tsunamis and floods to evaluate water-level deviations due to tsunamis traveling up rivers and from upstream flood flows. In addition to the 11 tsunami cases provided by the Central Disaster Prevention Council, calculations were performed for 55 cases considering five river flow patterns (base runoff, 25, 50, 75, and 100%) based on the most recent flood case in June 2023. The following conclusions were obtained:

(1) The Sana, Otowa, and Yagyu rivers exhibit the highest water level rises caused by tsunamis and flooding.

(2) When the flood scale is small, the rise in the water level at the river mouth is determined by the tsunami; therefore, the water level increases more at the river mouth. The flood is dominant when the most recent flood is assumed, and the water level rises farther upstream. However, when a flood is slightly smaller than that of the most recent flood (50% and 75%), the trends are divided into two categories depending on the tsunami case.

(3) When precipitation exceeds a certain amount during an earthquake, the water level rise characteristics can vary greatly and depend on the tsunami characteristics.

ACKNOWLEDGMENT

This research was supported by JSPS KAKENHI (Grants Nos. 23K13411, 23H00196). This work was conducted under Theme 4 of the Advanced Studies of Climate Change Projection (SENTAN Program) (Grant No. JPMXD0722678534), supported by the Ministry of Education, Culture, Sports, Science and Technology (MEXT), Japan.

REFERENCES

1. Aichi Prefecture: Mikawa Port BCP (Business Continuity Planning), 2015,pp 1-8, https://www.pref.aichi.jp/uploaded/life/360277_1517836_misc.pdf. Accessed 11, Dec 2024
2. Aichi Prefecture: Setting of normal river discharge in Toyo River, 2005,pp 1-11,https://www.pref.aichi.jp/uploaded/attachment/5924.pdf. Accessed 11,Dec 2024
3. Aoyama Y., A. Mohammad Bagu, Y. Mitobe, D. Komori, and H. Tanaka: Accuracy verification and characterization of numerical simulation of Tsunami run up into rivers. *Journal of Japan Society of Hydrology & Water Resources*, Vol. 30, No. 1, pp. 32–42, 2017
4. Baba T., A. Mikami, and M. Bando: A tsunami database created by using Earth simulator for real-time prediction, pp. 9–13, 2015.
5. Cabinet Office Central Disaster Prevention Council: Seismic intensity distribution and tsunami height due to a huge earthquake in the Nankai Trough (first report), Nankai Trough Huge Earthquake Model Review Committee, pp. 2–29, 2012.
6. Cabinet Office Central Disaster Prevention Council, Seismic Intensity Distribution, and Tsunami Height from a Huge Earthquake in the Nankai Trough (First Report), Nankai Trough Huge Earthquake Model Review Committee, pp. 2–29, 2012.
7. Cabinet Office Central Disaster Prevention Council: Estimated damage from a major earthquake in the Nankai Trough (Second Report), Central Disaster Prevention Council Disaster Prevention Measures Promotion Review Meeting, pp. 1–2, 2013.
8. Kayane K., H. Tanaka, and A. Mohammad Bagu: Influence of River Bed Slope for Tsunami Propagation into Rivers. *Journal of Japan Society of Civil Engineers, Ser. B2 (Coastal Engineering)*, Vol. 68, No. 2, I_176-I_180, 2012.
9. Kawasaki K., K. Myoungkyu, S. Shimokawa, and T. Murakami: Storm surge inundation prediction in Osaka port due to complex coastal disaster of huge earthquake and typhoon. *Journal of Japan Society of Civil Engineers, Ser. B3 (Coastal Development)*, Vol. 72, No. 2, I_13-I_18, 2016.
10. Kim S.Y., T. Yasuda, and H. Mase: Numerical analysis of effects of tidal variations on storm surges and waves. *Applied Ocean Research*, Vol. 30, pp. 311–322, 2008.
11. Ministry of Land, Infrastructure, Transport and Tourism: Guide to Setting Tsunami Inundation Projections - Coasts, p14-16, http://www.milt.go.jp/river/shishin_guideline/kaigan/tsunamishinsui_manual.pdf, Accessed 11,Dec 2024
12. Nakamura Y., T. Kakinuma, and T. Asano: A numerical simulation for the tsunami ascending rivers. *Journal of Japan Society of Civil Engineers, Ser. B2 (Coastal Engineering)*, Vol. 73, No. 2, I_331-I_336, 2017.
13. Sayama T., G. Ozawa, T. Kawakami, S. Nabesaka, and K. Fukami: Rainfall-Runoff-Inundation analysis of the 2010 Pakistan flood in the Kabul River basin. *Hydrological Sciences Journal*, Vol. 57, No. 2, pp. 298–312, 2012.
14. Tolkova E., H. Tanaka, and M. Roh: Tsunami Observations in Rivers from a Perspective of Tsunami Interaction with Tide and Riverine Flow. *Pure and Applied Geophysics*, Vol. 172, pp. 953–968, 2015.
15. Toyoda M., N. Mori, K. Sooyoul, Y. Shibutani, and J. Yoshino: Assessment of compound occurrence of storm surge and river flood in Ise and Mikawa Bays, Japan, using a framework of atmosphere–ocean–river coupling. *Nat Hazards* 120, 3891–3917 (2024).
16. Toyohashi City: Toyohashi City Nankai Trough Earthquake Damage Prediction Survey–Summary of Survey Results and Future Earthquake Disaster Prevention and Mitigation Measures, pp. 4–34, 2014.
17. Toyohashi City website: Toyohashi City Record of Heavy Rainfall in June 2023 (main text), pp. 1–7, 2023.
18. Yamazaki D., S. Togashi, A. Takeshima, and T. Sayama: High-resolution flow direction map of Japan. Journal of Japan Society of Civil Engineers (B1), Vol. 74(5), I_163-I_168, 2018.